Journal for ImmunoTherapy of Cancer

Perioperative pembrolizumab in early-stage non-small cell lung cancer (NSCLC): conventional and distribution-based immune profiling of the tumor microenvironment and peripheral circulation

Jingxuan Zhang,[1] Lin Lin,[1] Jennifer H Enzor,[2] Prekshaben H Patel,[2] Katelyn N Steadman,[2] Victoria E Little,[2] Lin Gu,[3] Eziafa I Oduah,[3] Betty C Tong,[4] Scott J Antonia,[3] Neal E Ready ,[3] Kent J Weinhold [2]

To cite: Zhang J, Lin L, Enzor JH, *et al*. Perioperative pembrolizumab in early-stage non-small cell lung cancer (NSCLC): conventional and distribution-based immune profiling of the tumor microenvironment and peripheral circulation. *Journal for ImmunoTherapy of Cancer* 2025;**13**:e012432. doi:10.1136/jitc-2025-012432

► Additional supplemental material is published online only. To view, please visit the journal online (https://doi.org/10.1136/jitc-2025-012432).

Accepted 07 October 2025

For numbered affiliations see end of article.

Correspondence to
Dr Kent J Weinhold;
kent.weinhold@duke.edu

ABSTRACT

Purpose A recently published phase 2 neoadjuvant trial in patients with early-stage non-small cell lung cancer (NSCLC) (NCT02818920) evaluated the potential efficacy of pembrolizumab administration in the absence of chemotherapy. This communication reports on conventional and distribution-based immune profiling efforts in efforts to identify novel biomarkers predictive of benefit.

Methods Patients with stage 1B-3A NSCLC received two cycles of pembrolizumab (P), followed by surgical resection of the remaining tumors (NCT02818920). Banked peripheral blood mononuclear cells (PBMCs) were analyzed at baseline and following the second dose of P. Resected tumors were disaggregated, and cells were viably cryopreserved. Based on pathologic examination of the tumors, patients were categorized as major pathologic responders (MPR; ≤10% viable tumor present), or non-MPR (>10% viable tumor present). High-parameter immune phenotyping by flow cytometry was performed on all available tumor and PBMC specimens, and results were expressed using both conventional phenotypic frequency analyses as well as a novel distribution-based biomarker identification strategy aimed at discovery of patterns associated with MPR.

Results Conventional, frequency-based flow cytometric immune phenotyping of participant tumor microenvironments and PBMC revealed several MPR-associated trends, only a few of which reached statistical significance. The distribution-based biomarker identification strategy greatly enhanced the discovery of statistically significant cell types and patterns of change associated with MPR.

Conclusions This novel, distribution-based analytic framework identified MPR-associated immune cell subsets in baseline PBMC that were not evident using conventional frequency-based immune profiling. Profiling the microenvironment of MPR-associated tumors revealed statistically significant distributional differences among highly expressed cellular markers on $CD8^+$ cells.

WHAT IS ALREADY KNOWN ON THIS TOPIC

⇒ Comprehensive profiling of immune cell populations within the tumor microenvironment and peripheral circulation of patients with non-small cell lung cancer (NSCLC) prior to and following neoadjuvant programmed cell death protein-1 (PD-1) administration can provide important insights into immune cell subsets associated with clinical outcomes following immune checkpoint immunotherapy.

WHAT THIS STUDY ADDS

⇒ Discovery of baseline biomarkers associated with major pathologic responses to neoadjuvant PD-1 checkpoint therapy remains an unmet clinical need. This novel distribution-based analytic platform identified highly significant baseline peripheral blood mononuclear cell immune cell subsets putatively associated with major pathologic responses following neoadjuvant pembrolizumab therapy.

HOW THIS STUDY MIGHT AFFECT RESEARCH, PRACTICE OR POLICY

⇒ This novel distribution-based analytic platform can be studied in larger immune profiling data sets of baseline and post-treatment blood from patients receiving neoadjuvant PD-1 checkpoint therapy for NSCLC. The analytic platform can be used to potentially identify additional immune cell subsets associated with benefit from PD-1 therapy. The identified immune cell subsets can be further studied in larger, independent data sets to establish baseline immune cell subsets predictive of response of patients with early NSCLC to PD-1 checkpoint therapy. If confirmed in future trials, these baseline predictive subset signatures could possibly be used to guide clinicians in identifying patients with early-stage NSCLC most likely to benefit from neoadjuvant PD-1 therapy in the absence of chemotherapy.

BACKGROUND

Non-small cell lung cancer (NSCLC) stands as a formidable global health challenge, consistently ranking among the leading causes of cancer-related mortality worldwide.[1 2] The emergence of immune checkpoint inhibitors (ICI) of the programmed cell death protein 1 (PD-1) for the treatment of advanced NSCLC has resulted in durable cancer control with an improvement in 5-year survival rates.[3–5] Adjuvant, neoadjuvant, and perioperative PD-1 checkpoint therapies have improved outcomes in early-stage NSCLC and have become standard of care in NSCLC without actionable molecular alterations prevalent in people who have never smoked.[6–8]

The effectiveness of immunotherapy in NSCLC varies considerably among individual patients, emphasizing the need for a deeper understanding of immune responses to the treatment intervention. Clinically, programmed death-ligand 1 (PD-L1) tumor proportion score (TPS) by immunohistochemistry (IHC) is used to predict responsiveness to immunotherapy in NSCLC.[9] However, PD-L1 IHC has considerable limitations as a diagnostic test. Although higher PD-L1 TPS scores have correlated with incremental responses in clinical trials of ICI in NSCLC, PD-L1 IHC positivity is predictive of response in less than 50% of patients.[10] Indeed, some PD-L1 negative tumors demonstrate response to immunotherapy, highlighting the complexity of the immune response to checkpoint blockade and the need for more robust understanding of the factors that lead to antitumor responses or resistance.[11] Consequently, immune profiling of the tumor microenvironment (TME) and peripheral blood to identify signatures of responses to immunotherapy is an active area of investigation in NSCLC.

Flow cytometry (FCM) is routinely used in cancer immunotherapy trials for monitoring the peripheral immune status of individual patients as well as the immune cell composition of the TME, providing detailed information on immune cell subsets, activation status, exhaustion, polyfunctionality, and other features. FCM is ideal for cellular immune biomarker discovery, enabling high-resolution insights into cellular characteristics and functional heterogeneities. FCM was used in a large phase 2 trial of neoadjuvant atezolizumab in NSCLC, and immune cell subsets were identified that were associated with response to atezolizumab.[7] Traditionally, biomarkers of an immune response are linked to the relative frequency of gated cell subsets, and to the abundance of specific cell surface or intracellular proteins within a gated cell subset. However, such frequency data can overlook differences in the biomarker distribution that can carry important information. For example, the overall frequencies can be the same between biomarkers with unimodal and bimodal distributions, biomarkers with left skew and right skew distributions, and biomarkers with low and high variance distributions. To address this limitation and gain a more comprehensive perspective on immune response biomarkers, we propose a distribution-based analysis using the Wasserstein distance to compare biomarker distributions and discover subtle details that we might otherwise miss when only using frequencies. Conceptually, the Wasserstein distance—arises from the idea of optimal transport—between two distributions A and B measures the minimal amount of work to shift probability mass so as to make A identical to B (or vice versa). Hence, the Wasserstein distance will identify potentially informative changes in biomarker distribution missed by frequency analysis.

The distribution-based analysis has also been used with single-cell RNA sequencing (scRNA-seq) data for differential expression analysis.[7 12–16] However, the high-throughput nature of FCM data, which can analyze millions of cells, poses a unique challenge for the implementation of distribution-based analysis. In this study, we propose a computational framework designed to facilitate efficient distribution-based analysis for FCM in cancer immunotherapy trials. This framework enables the comprehensive profiling of patients' immune status, allowing us to identify biomarkers associated with treatment responses and potentially predictive of those responses.

The Duke Cancer Institute phase 2 clinical trial TOP1501 is a multi-institutional phase 2 clinical trial (NCT02818920). Patients with stage 1B-3A NSCLC received two cycles of neoadjuvant pembrolizumab (P), surgery, chemotherapy, and adjuvant P. The clinical outcome of the patients enrolled in this trial has been recently reported.[17] Neoadjuvant trials such as this one present an opportunity to not only monitor immune subset changes in the peripheral circulation, but perhaps more importantly an opportunity to pathologically evaluate the relative percentages of remaining viable tumor cells and characterize the tumor immune microenvironment of the resection specimen obtained following the completion of immune checkpoint-based immunotherapy. Among the 25 patients undergoing tumor resections, 7 (28%) had major pathologic responses (MPR), wherein 10% or less viable tumor cells were present. This current report includes analysis of immunophenotyping data for the baseline and post second P peripheral blood mononuclear cell (PBMC) time point specimens as well as the resected tumor by traditional methods plus a novel distribution-based biomarker identification strategy to discover biomarkers associated with MPR following anti-PD-1 checkpoint therapy. We apply the proposed framework to analyze TOP1501 data and compare the results with those obtained using conventional methods.

METHODS

Patients

Eligible patients were 18 years or older with histologically proven clinical stage IB (tumor size >4 cm), II, or III (N0-N2) NSCLC as assessed according to the American Joint Committee on Cancer staging system, seventh edition deemed amenable to surgical resection. Eligibility criteria were typical for a lung cancer clinical trial, including

surgery and systemic therapy. Complete eligibility criteria have been published.[18] This protocol was approved by individual Institutional Review Boards (IRBs) in each of the participating centers. Each patient signed an IRB-approved, protocol-specific informed consent in accordance with federal and institutional guidelines.

Treatment

Patients received 200 mg intravenous P administered over 30 min for two 3 weeks/21 days cycles prior to surgery. Standard surgical evaluation was performed at least 21 days after the second dose of P along with repeat chest CT scan and reassessment by the treating medical oncologist. Surgery was performed at the discretion of the treating thoracic surgeon 29–56 days from the second dose of P per study protocol. After recovery from surgery, patients were re-evaluated by the treating medical oncologist and standard adjuvant chemotherapy was offered at their discretion. Postoperative radiation therapy was considered per institutional standard. Patients then received four additional cycles of adjuvant P every 3 weeks initiated 3–6 weeks after completion of all standard of care chemotherapy, and/or radiotherapy if given. To assess immunologic parameters, blood specimens were collected from each patient prior to beginning treatment, after cycle 2 of P prior to surgical resection, after surgery, and at the completion of all therapy. Following surgical pathology examination for standard of care tumor analysis, excess tumor was provided to the Duke Immune Profiling Core (DIPC) for disaggregation, viable cryopreservation, and subsequent immune profiling.

Methodologies

Collection and isolation of peripheral blood mononuclear cells

Blood was collected in tubes containing acid-citrate-dextrose anticoagulant (BD Vacutainer, Franklin Lakes, New Jersey, USA) and maintained at room temperature. PBMCs were separated by density gradient centrifugation using Lymphocyte Separation Medium (Corning, Tewksbury, Massachusetts, USA), washed, and counted, according to standard operating procedures (SOP) established in Substrate Services Core and Research Support laboratory at Duke University. PBMCs were subsequently resuspended in 90% fetal bovine serum (FBS; Gemini Bioproducts, Sacramento, California, USA) and 10% dimethylsulfoxide (DMSO; Sigma, St. Louis, Missouri, USA) solution, and progressively cooled overnight to −80°C and subsequently transferred to vapor phase liquid nitrogen for storage within 48 hours.

Tumor sample collection and processing

Following the Miltenyi Biotec Human Tumor Dissociation Kit protocol,[18] freshly isolated tumors, briefly held in MACS Tissue Storage Solution (Miltenyi Biotec), were dissociated into single-cell suspensions using Human Tumor Dissociation (enzymes (H, R, and A) Miltenyi Biotec) and gentleMACS processing equipment (Miltenyi Biotec). After two 30 min incubations at 37°C, the samples were filtered through a 70 µM filter (Corning) and washed in Roswell Park Memorial Institute (RPMI) 1640 (Thermo Fisher). Following centrifugation, the cells were resuspended in a 90% heat-inactivated FBS (Gem-Cell) and 10% DMSO (Sigma-Aldrich) solution, aliquoted into cryogenic vials and viably cryopreserved, and banked in vapor phase liquid nitrogen.

Flow cytometry staining

All flow cytometry assays were performed in the DIPC according to well-established SOP. All flow cytometry analyses were conducted in a strictly "blinded" manner whereby none of the DIPC personnel were aware of the clinical outcomes of each trial participant until after all the flow cytometry data were submitted and locked. Viably cryopreserved PBMC and tumor cell suspensions were thawed and washed in RPMI 1640 (Thermo Fisher) with 10% heat-inactivated FBS (Gem-Cell), 1% penicillin-streptomycin (Thermo Fisher), 1% L-glutamine (Thermo Fisher), and Benzonase (10 kU, Novagen) and counted following manufacturer's procedures using a Muse Cell Analyzer.[18] High parameter immune profiling was performed using a 22-channel T-cell Panel (online supplemental information table 1) and a 17-channel Innate/B–cell Panel (online supplemental information table 2) to profile PBMC subsets as well as components of the TMEs. Gating was performed according to best practices, with all gates set based on marker expression within a common batch control used across all four batches. The panel components as well as the detailed staining procedures are contained in the online supplemental information section of this report. These panels enabled the frequency quantification of multiple immune subsets, including T cells (cluster of differentiation (CD3)$^{+}$), T-helper ($CD4^{+}CD3^{+}CD8^{-}$), T-cytotoxic ($CD8^{+}CD3^{+}CD4^{-}$), regulatory T-cell (Treg) ($CD4^{+}CD25^{+}CD127^{low}$), T-cell maturation subsets (naive, central memory, effector memory, and effector), T-cell activation, T-cell exhaustion, tissue resident memory cells ($CD8^{+}$ $CD103^{+}CD366^{+}$), B cells ($CD19^{+}$), natural killer (NK) cells ($CD3^{-}CD16^{\pm}$ and $CD56^{\pm}$), monocyte subsets (classical monocytes: $CD14^{+}CD16^{-}$; non-classical monocytes: $CD14^{-}CD16^{+}$; and intermediate monocytes: $CD14^{+}CD16^{+}$), macrophages (M1: $CD68^{+}CD206^{-}$; M2: $CD68^{+}CD206^{+}$), and monocytic Myeloid-Derived Suppressor Cells (MDSC) ($CD11b^{+}CD15^{-}$HLA-$DR^{-}CD14^{+}$). It should be noted that, for TME profiling, only four MPR patient tumor specimens were available for T-cell profiling, three of which were also available for innate cell profiling. All graphic conventional flow cytometry data presented in figures 1 and 2, as well as online supplemental information figure 3 were constructed using Prism software (GraphPad) V.10.3.1.

Distribution-based differential expression analysis

Since PBMC samples were analyzed across multiple batches, we first performed batch effect correction to remove technical variations between different batches.

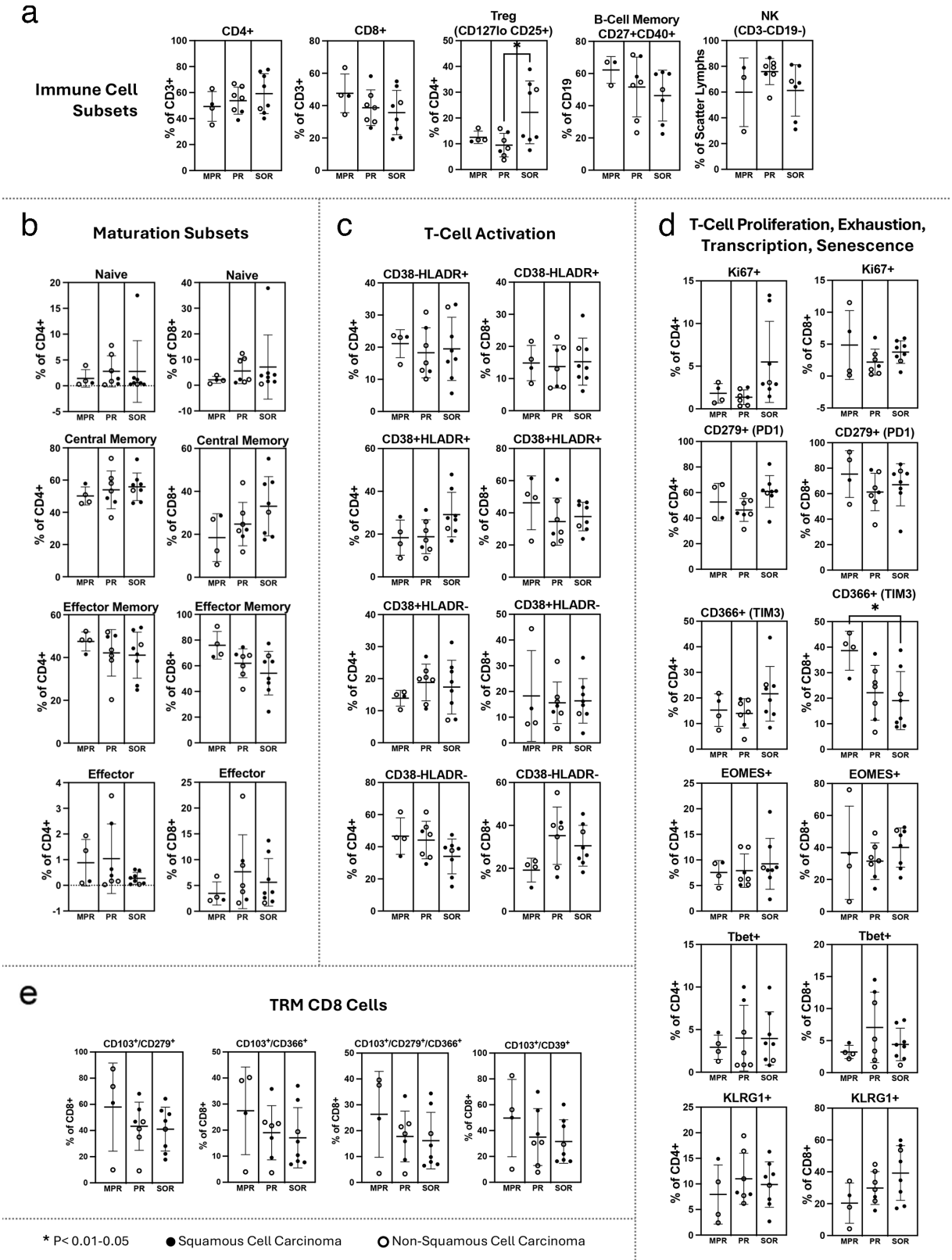

Figure 1 Conventional, frequency-based FCM immune profiling of the TME. EOMES (Eomesdermin), a T-box transcription factor; FCM, flow cytometry; HLA-DR, Human Leukocyte Antigen -DR isotype: KLRG1, killer cell lectin-like receptor subfamily G member 1; MPR, major pathologic responses; NK, natural killer; PD-1, programmed cell death protein 1; PR, pathologic response; SOR, suboptimal response; T-bet, a T-box expressed in T cells; TIM-3, T-cell immunoglobulin and mucin domain 3; TME, tumor microenvironment; Treg, regulatory T-cell; TRM, tissue resident memory.

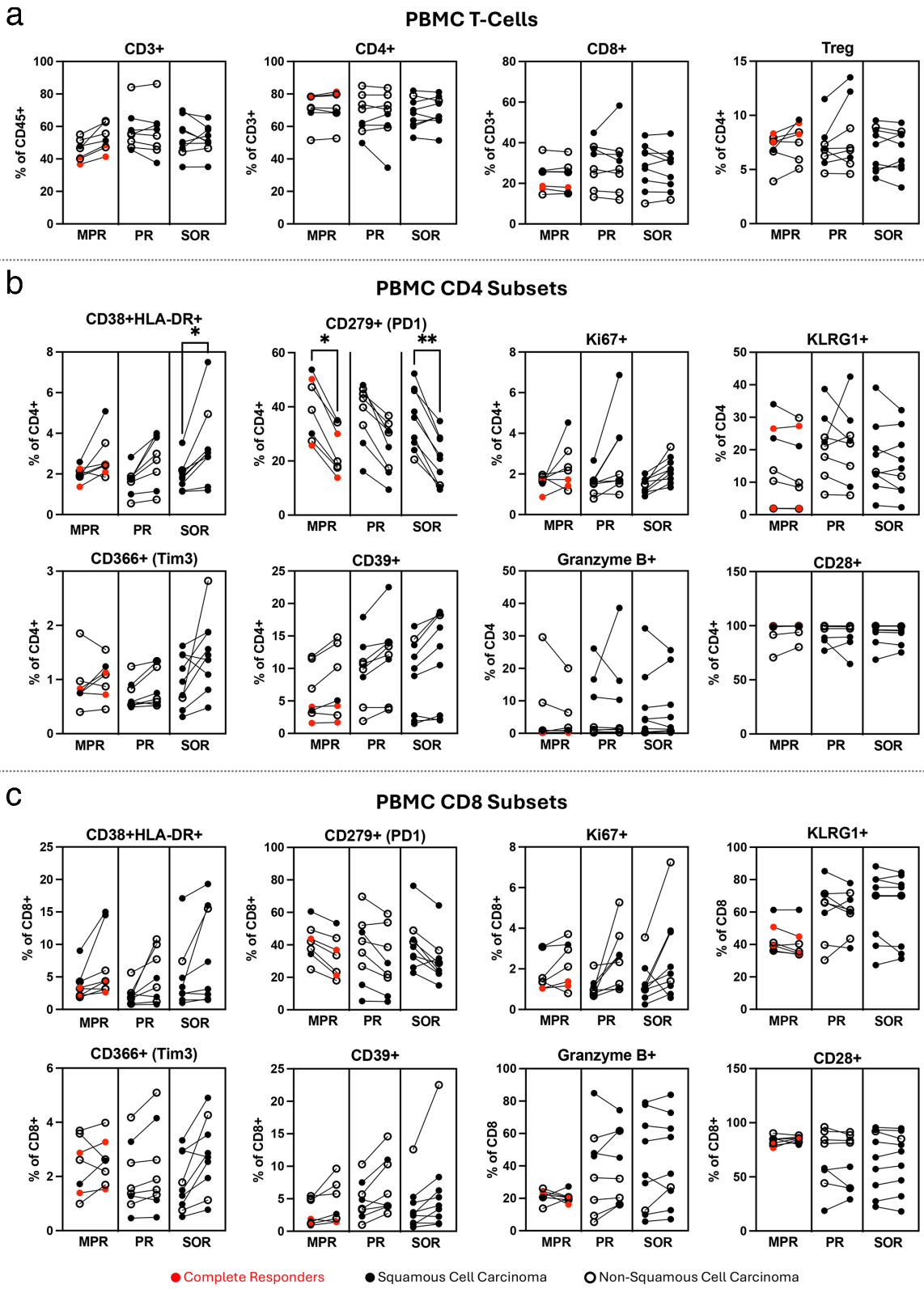

Figure 2 Conventional, frequency-based FCM immune profiling of the baseline and post-therapy PBMC. FCM, flow cytometry; HLA-DR, Human Leukocyte Antigen - DR isotype; KLRG1, killer cell lectin-like receptor subfamily G member 1; MPR, major pathologic responses; PBMC, peripheral blood mononuclear cell; PD-1, programmed cell death protein 1; PR, pathologic response; SOR, suboptimal response; TIM-3, T-cell immunoglobulin and mucin domain 3; Treg, regulatory T cell.

FCM data was first transformed using the standard biexponential function, and then alignment across batches was performed using the advanced statistical method: mutual nearest neighbors (MNN).[19] MNN identifies cells that are mutual nearest neighbors in the two datasets and then aligns one dataset with the other based on the observed

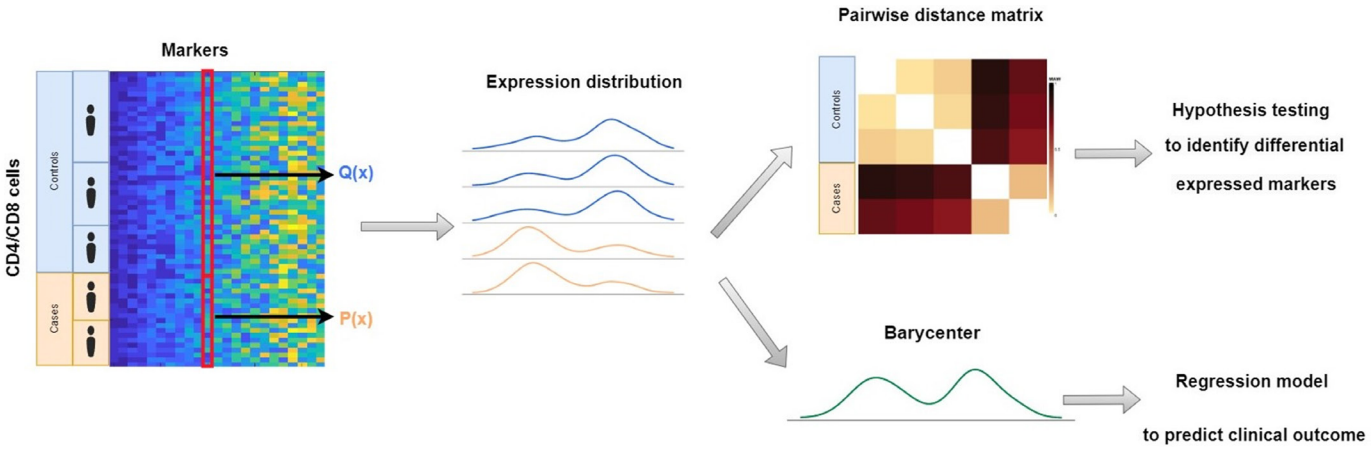

Figure 3 Overview of the pipeline for cytoDE and prediction analysis. The pipeline consists of multiple sequential steps beyond preprocessing, manual gating of cytometry data. Raw cytometry data should be preprocessed, including quality control, compensation, and transformation to normalize signal intensities before being imported to the model. Then a computational algorithm will be implemented based on minimized aggregated Wasserstein metric across each marker within each cell subpopulation in order to detect distributional difference between individuals. Inferential permutation hypothesis testing will lead to identifying differentially expressed markers between different groups of individuals while a regression model is established to predict clinical outcomes. cytoDE, cytometric differential expression.

differences in these identified pairs. This process helps correct for batch effect.

To identify biomarkers that discriminate between the MPR and non-MPR groups, we performed distribution-based differential expression (DE) analysis. First, for each cell type-specific marker, we modeled marker expression in individual patients as a probability distribution using Gaussian mixture models (GMMs). GMM is a widely adopted framework for model-based density estimation and clustering and has become an established paradigm for clustering FCM data.[20–24] This modeling allows us to capture not only differences in mean or median expression but also variability in distributional features such as variance, skewness, and multimodality. Subsequently, these GMM-based distributions were compared across individuals to identify differences between the MPR and non-MPR groups. However, classical statistical tests like the two-sample t-test and the Wilcoxon rank-sum test primarily detect shifts in central tendency (mean or median) and often lack sensitivity to more complex differences, such as variations in distribution shape or variance. Additionally, distribution-based DE methods developed for scRNA-seq data are not directly transferable to FCM data due to differences in data characteristics and scale. Therefore, we developed and applied cytometric DE (cytoDE), a distribution-based DE analysis specifically designed for FCM data, for the DE analysis. As illustrated in figure 3, cytoDE conducts DE testing, marker by marker, for a given cell type with respect to a grouping variable—in our case, MPR versus non-MPR. The cytoDE pipeline involves three main steps: (1) Construction of GMMs: for each marker and each patient, cytoDE fits a GMM to the marker's expression data. This step models the distributional characteristics of the data, capturing complex features such as multimodality, skewness, and variance that go beyond simple summary statistics like the mean. (2) Distance calculation: using the fitting GMMs, cytoDE computes pairwise distances between patients' marker expression distributions. This is accomplished with our computationally efficient minimized aggregated Wasserstein (MAW) distance algorithm for GMMs,[25] which quantifies differences in the entire distributional shape. (3) Statistical testing: from the resulting pairwise distance matrix, cytoDE tests whether patients within the same group (MPR or non-MPR) have more similar distributions compared with patients from different groups. This is assessed using a distance-based Welch t-test,[26] producing a p value for each marker to quantify the statistical significance of distributional differences between groups. Through this approach, cytoDE offers enhanced sensitivity for detecting subtle yet biologically meaningful differences that traditional tests might overlook. Additional details about the cytoDE method and its benchmarking against conventional statistical approaches are provided in the online supplemental information. The code for implementing the distribution-based differential expression (DE) analysis is available at https://github.com/llin-lab/cytoDE.

Distribution-based predictive analysis

After computing the distances between biomarker distributions, we identify the corresponding centroid of the patient-derived distributions, known as the MAW barycenter. Our predictive approach then leverages the distance between each patient's distribution and the MAW barycenter as a key covariate in logistic regression models to predict patient outcomes.

This distance is proposed as a potential feature for predicting patient outcomes for several reasons: (1) enhanced sensitivity to subtle variations: this distance, by computing differences in distribution patterns, has the potential to capture nuanced variations within the

patient sample; (2) interpretable insight into distribution variation: this distance provides interpretable insight into the variation within patient distributions, as it essentially reflects how each patient's distribution deviates from the centroid, offering a measure of data heterogeneity; and (3) seamless integration into prediction models: as the distance is a scalar quantity, it can be easily integrated into various prediction models, facilitating its use across different analytical frameworks. The pipeline is illustrated in figure 3, and details on the predictive analysis are provided in online supplemental information.

RESULTS

Patient characteristics and treatment

Between April 10, 2017, and February 6, 2019, 35 patients provided informed consent and 30 patients received study therapy. Demographic characteristics of patients enrolled of note included: male (16, 53%), white (29, 97%), median age 72 years (range 47–81), current or former people who smoke (26, 87%), and squamous histology (17, 57%). Nine patients (30%) had stage IB disease, seven patients (23%) had stage IIA disease, six patients (20%) had stage IIB disease, and eight patients (27%) had stage IIIA disease. Of the 30 patients who received neoadjuvant P, 5 were not deemed to be candidates for surgical resection due to 4 stage IIIB discovered at surgery and 1 disease progression. Of the 25 patients who underwent surgical resection of their lung cancer, 19 had available excess tumor with collection of viable cells adequate for profiling, while 6 cases, including 2 cases with complete response and 1 with MPR, had no excess adequate tumor available after tumor was taken for standard pathologic testing. An MPR, defined as less than or equal to 10% of viable tumor remaining at time of surgery, was observed in seven specimens (28%). This included four specimens with adenocarcinoma histology, two with squamous histology, and one with adeno-squamous histology. Two specimens (8%) were observed to have complete pathologic response of which both had squamous histology documented before initiation of therapy. The higher rate of MPR in non-squamous NSCLC compared with squamous lung cancer was not seen in a larger study of perioperative atezolizumab in NSCLC, so the increased MPR rate in non-squamous histology may be due to small sample size.[7]

Conventional phenotypic frequency analyses

Tumor microenvironment profiling

The 19 available resected patient tumors (4 MPR all progression-free and 15 non-MPR 12 (80%) progression-free) were profiled for immune cell (ie, CD45+) phenotypic subset frequencies. Once again, based on pathologic examination of the resected tumors, patients were categorized as MPRs (≤10% viable tumor present) or non-MPR (>10% viable tumor present). Given the relatively small sample sizes, many potential differences in expression frequencies represent trends which may be better revealed using additional subclassifications of the non-MPR group. To provide additional insights into the possible relationship between immune subset profiles and relative viable tumor burden, non-MPR tumors were further subclassified into two additional groupings based on the pathologic estimates of viable tumor cell percentages present as was done on a large trial studying perioperative atezolizumab in NSCLC.[7] Tumors estimated as harboring 11–50% viable tumor cells were classified as "Pathologic Response" (PR) 5/7 (71%) progression-free, while those tumors estimated with >50% viable tumor cells were classified as "Sub-Optimal Response" (SOR) with 7/8 (87%) progression-free. PR rate in this study was associated with response to P alone while progression-free survival was influenced by surgery, and adjuvant chemotherapy in addition to P. Representative data sets of interest are presented in figure 1. Regarding tumor-associated T cells, there appears to be an overall trend wherein MPR tumors harbor the lowest mean $CD4^+$ cell frequencies compared with "PR" and "SOR" tumors, and highest mean $CD8^+$ frequencies among the three groups (figure 1a). Mean Treg frequencies were highest among the "SOR" tumor group, while mean memory B-cell frequencies trended highest among MPR, possibly reflective of terminal lymphoid structures present. No discernible differences in mean NK cell frequencies were noted among the three groups. Regarding T-cell maturation subsets (figure 1b), "SOR" tumors trended highest frequencies of $CD8^+$ central memory cells, while $CD8^+$ effector memory frequencies trended highest among MPR tumors. In the context of T-cell activation (figure 1c), "SOR" tumors harbored highest frequencies of CD38/HLA-DR double positive $CD4^+$ cells, while MPR tumors maintained lowest frequencies of CD38/HLA-DR double negative $CD8^+$ cells. Tumor-associated $CD8^+$/killer cell lectin-like receptor subfamily G member 1 $(KLRG1)^+$ cell frequencies trended lowest among MPR tumors and highest among "SOR" tumors (figure 1d), suggesting a possible relationship between senescence and tumor burden. Among the most interesting findings was the significantly greater frequency of T-cell immunoglobulin and mucin domain 3 (TIM-3) (CD366) positive $CD8^+$ cells among the MPR tumors (figure 1d). The data in figure 1e reveal increased frequencies of $CD8^+$/$CD279^+$, $CD8^+$/$CD366^+$ cells as well as $CD8^+$/$CD279^+$/$CD366^+$ co-expressing cells among MPR tumors, all in conjunction with the tissue resident marker CD103, consistent with a previous report that tissue resident $CD8^+$ cells co-expressing PD-1 and TIM-3 were enriched in lung cancer responders to PD-1 inhibitors, and highlighting that not all $PD\text{-}1^+$ potential cytotoxic T cell (CTL) effectors are dysfunctional.[27] Also depicted in figure 1e is the high frequency of $CD8^+$/$CD103^+$ cells among MPR tumors that express CD39, another putative exhaustion marker that marks potential antitumor effectors. In contrast to the noted trends among adaptive immune cell subsets, few specific innate subsets trended among the three tumor groupings (online supplemental information figure 3).

Peripheral blood mononuclear cell profiling

A total of 24 paired baseline and post second P dose PBMCs were available for flow-based immune profiling, including samples from the two complete responders among the total of seven MPRs. An extended data set can be found in the online supplemental information section of this communication. The data depicted in figure 2a reveal generally similar $CD3^+$ $CD4^+$ and $CD8^+$ T-cell subset frequencies, as well as Tregs, comparing PBMC from among MPR, PR, and SOR patients (figure 2a). The significant decreases in post-treatment frequencies of CD279-expressing CD4+ cells and, to a lesser extent $CD8^+$ cells (figure 2b), for both MPR, PR, and SOR PBMC samples are, most likely, due to blocking of cell surface CD279 staining in these samples that were obtained shortly after the second dose of P. Granzyme B $(GZMB)^+$ $CD8^+$ cells generally trended lower, while CD28 expression among $CD8^+$ cells remained uniformly high within the MPR group, while appearing highly variable within the PR and SOR groups (figure 2c). Among non-lymphocyte populations, the only noteworthy change was a complete reversal in macrophage phenotype in the PBMC of one of the MPR patients from approximately 70% M2 subtype present at baseline to 80% M1 phenotype following the second dose of P (online supplemental information figure 3C). Despite our extensive efforts to identify statistically significant baseline PBMC immune signatures unique to MPR patients by conventional flow cytometry-based frequency profiling, none were found.

Distribution-based differential expressed analysis

TME profiling

We first applied cytoDE to the tumor samples, analyzing 70 cell subsets obtained from manual gating and 19 markers. DE markers with p values below 0.05 are reported in online supplemental information table 3. As this is an exploratory study, we did not apply multiple testing corrections, opting to present raw p values instead. Our DE analysis revealed a significant difference in CD39 expression among $CD8^+$ cells between the MPR and non-MPR groups. Figure 4a shows the density plots of CD39 expression levels in $CD4^-$ $CD8^+$ T cells, color-coded by patients and stratified into two groups: MPR (left panel) and non-MPR (right panel). The density plots enable a comparative analysis of the heterogeneity in CD39 expression between the two groups. While both groups exhibit (roughly) bimodal distributions of CD39 expression, the MPR group displays a lower density at the lower expression levels of CD39 compared with the non-MPR group, which also shows higher variability in the distribution overall. In addition to the frequency analyses, we performed a Wilcoxon test to compare the mean CD39 expression between the MPR and non-MPR groups in $CD4^-$ $CD8^+$ T cells (figure 4b). The test yielded a p-value of 0.02, consistent with the findings from our cytoDE analysis.

In addition to CD39, our cytoDE analysis also identified CD366 (TIM-3) as a novel DE marker within $CD4^-$ $CD8^+$ cells. Figure 4c presents the density plots of CD366 expression levels in $CD4^-$ $CD8^+$ T cells across patients, displaying a similar bimodal pattern to that observed in figure 4a. However, the two peaks (modes) in figure 4c

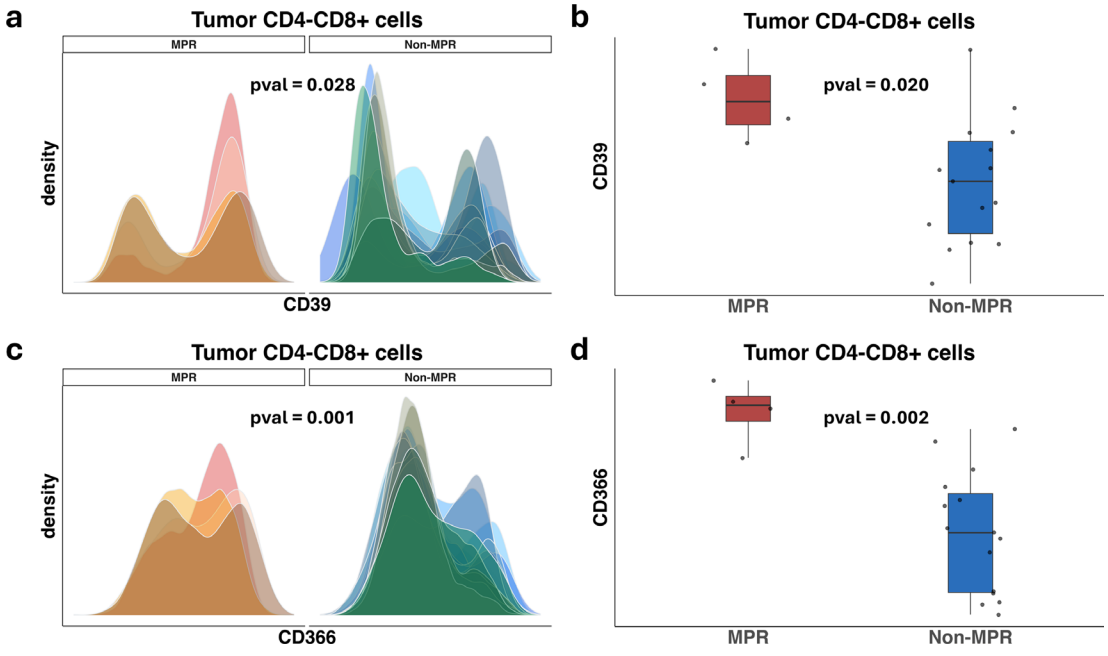

Figure 4 Tumor distributional-based test result. Subplots (a) and (c) display density plots of CD39 and CD366 expression within CD8+ cells in tumor samples, illustrating distinct expression distribution patterns between patients in the MPR and other/SOR groups. Subplots (b) and (d) use traditional boxplots to confirm that the means of marker expression differ significantly between the two groups. CD, cluster differentiation; MPR, major pathologic responses; SOR, suboptimal response.

are less distinct and show less separation compared with figure 4a. Specifically, the MPR group exhibits a less pronounced peak at the lower CD366 expression levels, while the non-MPR group shows a higher concentration of cells with CD366 expression in the lower expression region. Figure 4d also confirmed this finding by comparing the mean CD366 expression within $CD4^-$ $CD8^+$ T cells for each patient between MPR and non-MPR groups. TIM-3, a membrane protein in the immunoglobulin and mucin domain-containing family, was initially discovered in terminally differentiated interferon-γ-producing Th1 (T helper) and Tc1 (T cytotoxic) murine cells and later shown to regulate Th17 cells in humans.[28] Gautron *et al*[28] demonstrated that TIM-3 enhances the suppressive function of $FoxP3^+$ Tregs on Th1 and Th17 responses. Additionally, TIM-3 is expressed on tumor-infiltrating dendritic cells, where it suppresses antitumor immunity. However, the precise role of the TIM-3/phosphatidylserine axis in cancer progression remains unclear.

Baseline PBMC profiling

We focused on $CD4^-$ and $CD8^+$ T cells, with manual gating identifying 28 $CD4^-$ subsets and 19 $CD8^+$ subsets. DE analysis was performed comparing the MPR and non-MPR groups for all subsets and markers, with DE markers having raw p values below 0.05 reported in online supplemental information table 4. Conventional analysis identified trending differences in the proportions of $GZMB^+$ and $KLRG1^+$ $CD8^+$ cells. Our DE analysis further revealed significant differences in the expression distributions of GZMB and KLRG1 specifically within the $CD8^+$ $CD45RA^+$ $CD197^+$ naïve T-cell subset, comparing PBMCs from MPR versus non-MPR patients (figure 5a and c). These findings highlight that in the MPR group, this $CD8^+$ cell subpopulation tends to exhibit lower expression levels of GZMB and KLRG1, a trend consistent with the conventional analysis (figure 5b and d). Interestingly, when comparing mean GZMB expression levels within $CD8^+$ cells using the Wilcoxon test, the resulting p value was 0.11, indicating no statistically significant difference between the two groups. This lack of significance may be attributed to the fact that, while the non-MPR group includes a subset of cells with high GZMB expression, the proportion of these cells is not large enough to impact the mean expression level. As a result, the mean value fails to capture the distributional differences that our DE analysis detected.

These findings point to the potential functional consequences of lower GZMB and KLRG1 expression in $CD8^+$ cells, which may have important implications for immune responses in cancer. In particular, diminished GZMB expression could affect the ability of T cells to effectively kill tumor cells, a key mechanism in immune-based therapies.

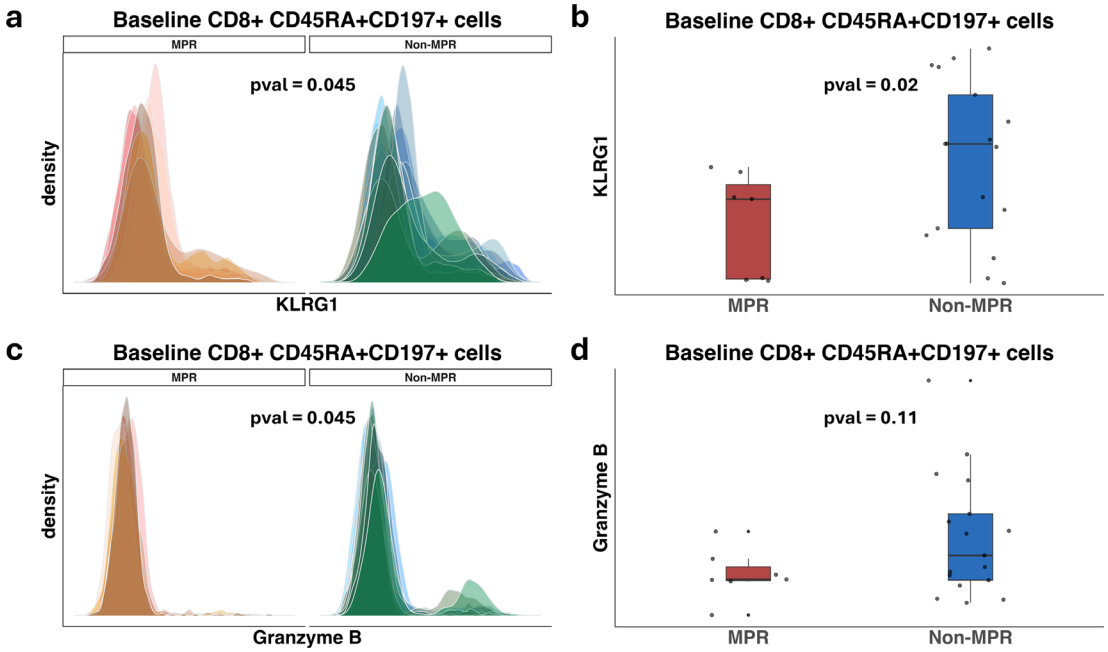

Figure 5 Baseline PBMC distributional-based test result. Subplots (a) and (c) display density plots of KLRG1 and granzyme B expression within CD8+CD45RA+CD197+ cells in samples at baseline study, illustrating distinct expression distribution patterns between patients in the MPR and other/SOR groups. Subplots (b) and (d) use traditional boxplots to show the means of marker expression between the two groups. Although KLRG1 provides a consistency in the hypothesis testing conclusion based on the two subplots (a) and (b), granzyme B fails to be identified as the differentially expressed marker using only traditional analytic methods when comparing the first moment of the expression level. This might be because the only significant distinction occurred on the overlooked right region (high expression peak) but not the heavy weight on the left region (low expression peak). CD, cluster differentiation; KLRG1, killer cell lectin-like receptor subfamily G member 1; MPR, major pathologic responses; PBMC, peripheral blood mononuclear cell; SOR, suboptimal response.

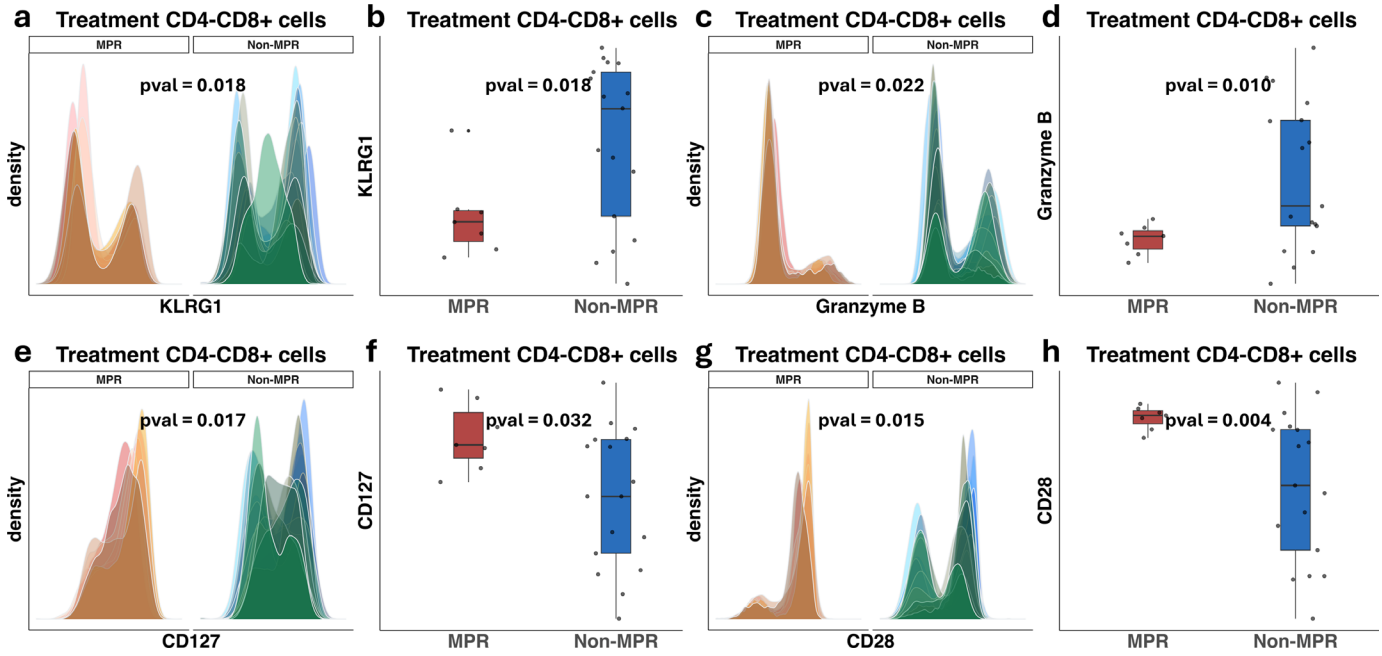

Figure 6 Treatment PBMC distributional-based test result. Subplots (a) and (c) display density plots of KLRG1 and granzyme B expression within CD8+ cells in samples after treatment study, illustrating distinct expression distribution patterns between patients in the MPR and other/SOR groups. Subplots (b) and (d) use traditional boxplots to confirm that the means of marker expression differ significantly between the two groups. Subplots (e) and (g) display density plots of two additional differentially expressed markers, CD127 and CD28, within CD8+ cells in samples after treatment study, illustrating distinct expression distribution patterns between patients in the MPR and other/SOR groups. Subplots (f) and (h) are the corresponding boxplots based on the expression means across each individual in order to confirm that the means of marker expression differ significantly between the two groups. CD, cluster differentiation; KLRG1, killer cell lectin-like receptor subfamily G member 1; MPR, major pathologic responses; PBMC, peripheral blood mononuclear cell; SOR, suboptimal response.

Treatment PBMC profiling

DE markers having raw p values below 0.05 are reported in online supplemental information table 5. Figure 6a, c show a significant difference in the expression levels of GZMB and KLRG1 on $CD8^+$ T cells, as well as in most CD8+ subpopulations between the MPR and non-MPR groups. Specifically, the MPR group exhibited lower overall expression levels of both markers in this $CD8^+$ subpopulation. These findings align closely with the results of the conventional analysis and when comparing mean expressions (figure 6b, d). Additionally, our analysis identified CD127 and CD28 as DE markers in $CD8^+$ cells (figure 6e and g) their subpopulations, based on the relevant gating strategies (online supplemental information table 5). These results were further validated using the Wilcoxon test on the mean expression values, confirming the significance of the differences (figure 6f and h). Interestingly, both markers were found to be upregulated in the MPR group.

Distribution-based predictive analysis

We applied our distribution-based predictive approach to identify potential biomarkers associated with predicting patient outcomes. The analysis was performed in two stages: first, using only baseline PBMC data, and second, integrating both baseline and treatment PBMC data. Figure 7a illustrates the receiver operating curve (ROC) curves from leave-one-out cross-validation, highlighting the five most predictive markers derived from baseline data, ranked by their area under the curve (AUC) values. Similarly, figure 7b presents the ROC curves for the top five predictive markers when both baseline and treatment data were incorporated.

These figures reveal markers with strong predictive performance, where higher AUC values suggest their potential utility for predicting patient outcomes. Notably, CD25 within $CD8^+CD45RA^+CD197^+$ T cells from the baseline data achieved the highest AUC of 0.82. However, this AUC dropped significantly to 0.46 and 0.48 when only a single covariate—either the distance term or the optimal transport matrix term—was included in the regression model, suggesting the importance of both terms as covariates in predicting outcomes. When incorporating both baseline and treatment data (figure 7b), CD197 within $CD8^+$ $CD39^+$ T cells emerged as the most predictive marker, achieving an AUC of 0.90. In contrast, when limiting the model to only the distance terms and optimal transport matrix terms, the AUC dropped sharply to 0.22 and 0.47, respectively.

DISCUSSION/CONCLUSION

This study advances our understanding of the immune landscape in early-stage NSCLC treated with neoadjuvant PD-1 checkpoint-based therapy in the absence of chemotherapy by identifying key immune markers and

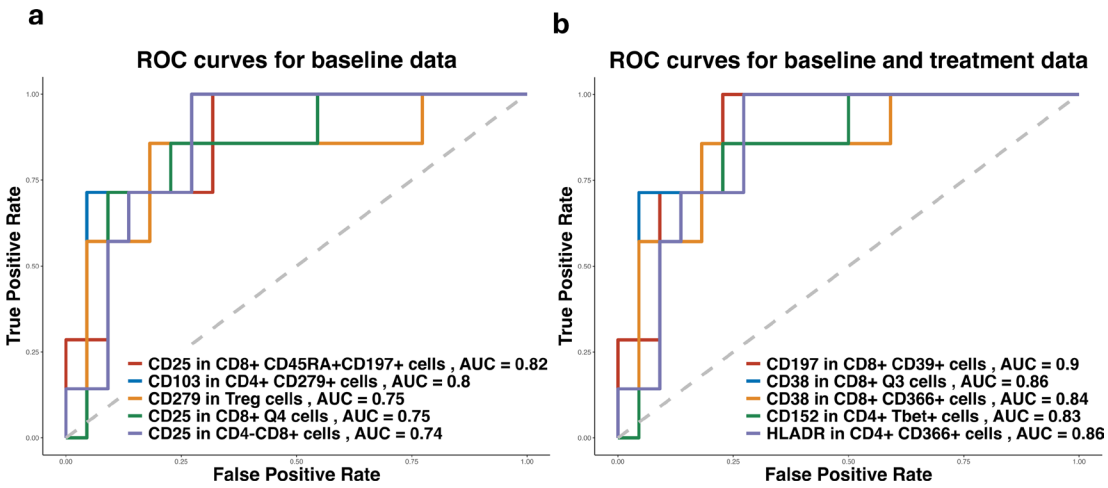

Figure 7 Predictive analysis. Subplot (a) displays the ROC curve of the predictive regression model using baseline data for single marker within certain cell subpopulation, while subplot (b) displays the ROC curve of the model using both baseline and predictive data for single marker within the cell subpopulation. AUC, area under the curve; CD, cluster differentiation; HLA-DR, Human Leukocyte Antigen -DR isotype; Tbet, T-box expressed in T cells, ROC, receiver operating curve; Treg, regulatory T-cell.

subpopulations that distinguish MPR from pathologic non-responders. By combining conventional flow cytometry frequency-based analyses with our novel distribution-based differential expression strategy (cytoDE), we revealed statistically significant distinct immune signatures within both the TME and peripheral blood, offering valuable insights into the determinants of therapeutic response.

Within the TME, we observed unique patterns of CD39, CD279 (PD-1), and CD366 (TIM-3) expression on $CD8^+$ T cells, all of which have been regarded as markers of T-cell exhaustion. Initially surprised by the high frequencies of TIM-3^+ $CD8^+$ T cells populating the TME of MPR patients (figure 1d), a review of the recent literature revealed emerging evidence that a subpopulation of these CD103+/$CD8^+$ tissue resident memory (TRM) T cells that co-express PD-1, TIM-3 and/or CD39 are actually associated with improved prognosis and better clinical outcomes for a variety of human tumors[27–34] including patients with NSCLC receiving immune checkpoint therapies.[35] Classically regarded as terminally exhausted cells incapable of measurable effector activities, at least one report categorized these as “progenitor exhausted” cells that are long-lived, respond to anti-PD-1 therapy, and retain polyfunctionality as they control tumor growth.[36] These cells are believed by some to represent actual antitumor effectors, and associate with improved Overall Survival (OS) among patients receiving ICI therapies. Notably, MPR patient tumors exhibited higher frequencies of $CD8^+$ expressing CD39 and TIM-3, but lower densities and levels of CD39 and TIM-3, suggesting a less exhausted TME conducive to better antitumor responses. Previous research has shown that signatures of heterogeneous tumor-infiltrating tissue-resident memory TRM and “pre-exhausted” long-lived effector-memory $CD8^+$ T cells are associated with improved responses to immune checkpoint blockade therapy, but only in the presence of CD28. This suggests that CD28 may play a critical regulatory role in the TME of lung cancer.[37] Additionally, interleukin-7 stimulation has been demonstrated to increase total CD127 messenger RNA expression and promote the release of sCD127 by $CD8^+$ T cells, which in turn enhances the functionality of mature and immature T cells, as well as immature B-cell proliferation and development.[38] Different from conventional frequency-based testing, our distribution-based analysis evaluates each marker expression within each cell subset, leading to a greater number of hypotheses to be tested. In our analysis, we did not apply multiple testing adjustments, as this is an exploratory study.

A number of previous studies, including a few focused on NSCLC, have attempted to identify PBMC signatures that predict responsiveness to immune checkpoint therapies,[39–43] although no consistent findings across these studies were readily apparent. Unlike the present study, most involved immunotherapies or chemo-immunotherapies in advanced stage patients. Ichiki *et al* reported that changes in the frequencies of PBMC-associated $CD103^+CD39^+CD8^+$ cells following ICI monotherapy administration may predict efficacy.[39] In our present study of patients with NSCLC, this specific cell population was relatively abundant within the TME (figure 1e), with highest mean frequencies among MPR patients, but extremely rare among baseline and on-therapy PBMC of all three groups (data not shown), perhaps owing to the early stage of our current participants. Miao and colleagues suggested that baseline frequencies of $CD4^+CD45RA^-$ T cells may predict ICI efficacy, while $CD8^+CD38^+$ frequencies may be suggestive of immune-related adverse events.[40] In contrast, Chaft *et al* concluded that significant expansion of activated $CD8^+$ was observed in patients demonstrating MPR.[7] In a chemoimmunotherapy study of patients with advanced pleural mesothelioma, Chin *et al* reported that $CD8^+$ effector memory T cells with stem-like properties were more frequent at baseline in responders, and continued

to expand on treatment.[41] In their review, Marcos Rubio *et al* concluded that "…there are no cell subpopulations yet that can solely predict the outcome of ICI-treated NSCLC patients and replace PD-L1 expression testing as the standard clinically available option".[42] Most recently, Kim *et al*, using an scRNA-seq platform on baseline PBMC samples, reported that the presence of $CD4^+$ and $CD8^+$ T cells with perforin and *GZMB* expression showed strong associations with favorable prognosis, while serious adverse events were associated with monocytes and macrophages.[43] In our present flow cytometry-based study of patients with early-stage NSCLC, no significant predictive baseline or post-therapy PBMC subset frequencies were apparent.

However, in our distribution-based PBMC analyses, we identified significant differences in key markers—GZMB, KLRG1, CD127, and CD28—across $CD8^+$ T-cell subsets. The reduced expression of the cytotoxic marker GZMB in MPR patients, while seemingly counterintuitive, may reflect a transition toward a "pre-exhausted" T-cell state that favors sustained immune responses. Concurrent upregulation of CD127 and CD28 further underscores the importance of functional memory T cells in driving durable antitumor immunity and improved responses to PD-1 blockade. The reduced effector function of activated T and NK cells may contribute to diminished tumor cell death, even when these cells are no longer inhibited by immune checkpoints. Disruption of GZMB activity could result in reduced cell entry, trafficking, or accumulation within the cytoplasm of target cells, such as tumor cells. Alternatively, it may be linked to decreased enzymatic activity, reducing the cleavage of intracellular substrates required for tumor cell death.

These findings carry significant clinical implications. If validated in larger, independent cohort studies GZMB, CD127, and CD28 levels in baseline PBMCs hold potential promise as predictive biomarkers for stratifying patients with early NSCLC most likely to benefit from neoadjuvant immune checkpoint therapy in the absence of chemotherapy. Such biomarkers could inform precision treatment strategies, improving patient outcomes while minimizing unnecessary interventions.

The clinical outcomes of patients enrolled in this trial have been previously reported.[17] There was a trend towards higher PD-L1 TPS scores in patients who demonstrated an MPR postoperatively; however, it did not reach statistical significance. Although this could be due to the small numbers of patients, it may also be reflective of the limitations of PD-L1 alone as a biomarker of response to immune checkpoint inhibition. Future studies should focus on validating these immune signatures across diverse patient populations and correlating them to known biomarkers such as PD-L1 TPS and other molecular mechanisms of resistance or response to checkpoint blockade. It is also critical to elucidate their functional roles in NSCLC progression and response to therapy. Integrating these biomarkers into clinical workflows has the potential to enhance the precision of immune-based therapies, paving the way for broader adoption of personalized oncology in the management of early-stage NSCLC.

Author affiliations
[1]Department of Biostatistics and Bioinformatics, Duke University School of Medicine, Durham, North Carolina, USA
[2]Division of Surgical Sciences, Department of Surgery, Duke University School of Medicine, Durham, North Carolina, USA
[3]Division of Medical Oncology, Duke University Health System, Durham, North Carolina, USA
[4]Division of Cardiovascular Cardiovascular and Thoracic Surgery, Duke University Health System, Durham, North Carolina, USA

Acknowledgements The authors acknowledge the technical support provided by the Duke Immune Profiling Core (DIPC) a Duke Department of Surgery-supported, Duke School of Medicine designated Service Center, and NIH-sponsored Duke Cancer Institute Shared Resource (NIH-2P30CA014236). Non-author contributions to this work include the thoracic oncology clinical research teams at participating institutions (Duke, Dartmouth, and Mayo Clinic), as well as the assistance of Lauren Halligan, CMI, in constructing composite data figures 1 and 2, as well as online supplemental information figure 3. Lastly, the authors gratefully recognize all participants in this multi-institutional phase 2 clinical trial (NCT0281890).

Contributors JZ and LL performed all of the distribution-based analyses of the FCM data and provided the associated narratives. JHE, PHP, KNS, and VEL performed the flow cytometry assays according to best practices, and JHE performed all of the conventional FCM data analyses. KJW oversaw all of the conventional FCM assay performance and conventional data analyses, organized and presided over all in-person and virtual meetings among co-investigators, assumed responsibility for initial and subsequent manuscript drafts, and was responsible for final manuscript submission and communication with the journal staff, all coauthors, including the aforementioned and EIO, BCT, LG, SJA, NER, and KJW provided substantial contributions to the conception, analysis, and interpretation of the data for this work, in addition to efforts related to drafting, reviewing the final version for publication, and agreeing to be accountable for all aspects. The guarantor of this work is NER. The corresponding author's email address is kent.weinhold@duke.edu. The corresponding author's mailing address is P.O. Box 2926, Duke University Medical Center, Durham, North Carolina, USA, 27710-2926.

Funding Merck Sharp & Dohme LLC, a subsidiary of Merck & Co., Inc., Rahway, New Jersey, USA, provided financial support for the study. The opinions expressed in this paper are those of the authors, and do not necessarily represent those of Merck Sharp and Dohme LLC. The data presented in this communication were derived from patients enrolled in an investigator-initiated trial where study design, data collection, analysis, interpretation of data, report writing, and decision to submit for publication were managed by NR without sponsor influence.

Competing interests None declared.

Patient consent for publication Not applicable.

Ethics approval This study involves human participants and was approved by Duke University Institutional Review Board: Duke Pro00071629.

Provenance and peer review Not commissioned; externally peer reviewed.

Data availability statement Data are available upon reasonable request. The data (de-identified participant data) generated in this study are available upon request from the corresponding author, KW.

ORCID iDs
Neal E Ready https://orcid.org/0000-0003-4414-9432
Kent J Weinhold https://orcid.org/0000-0003-4876-6737

REFERENCES

1 Felip E, Altorki N, Zhou C, *et al*. Overall survival with adjuvant atezolizumab after chemotherapy in resected stage II-IIIA non-small-cell lung cancer (IMpower010): a randomised, multicentre, open-label, phase III trial. *Ann Oncol* 2023;34:907–19.
2 Wakelee H, Liberman M, Kato T, *et al*. Perioperative Pembrolizumab for Early-Stage Non-Small-Cell Lung Cancer. *N Engl J Med* 2023;389:491–503.
3 Provencio M, Nadal E, González-Larriba JL, *et al*. Perioperative Nivolumab and Chemotherapy in Stage III Non-Small-Cell Lung Cancer. *N Engl J Med* 2023;389:504–13.
4 Heymach JV, Harpole D, Mitsudomi T, *et al*. Perioperative Durvalumab for Resectable Non–Small-Cell Lung Cancer. *N Engl J Med* 2023;389:1672–84.
5 Forde PM, Spicer J, Lu S, *et al*. Neoadjuvant Nivolumab plus Chemotherapy in Resectable Lung Cancer. *N Engl J Med* 2022;386:1973–85.
6 Forde PM, Chaft JE, Smith KN, *et al*. Neoadjuvant PD-1 Blockade in Resectable Lung Cancer. *N Engl J Med* 2018;378:1976–86.
7 Chaft JE, Oezkan F, Kris MG, *et al*. Neoadjuvant atezolizumab for resectable non-small cell lung cancer: an open-label, single-arm phase II trial. *Nat Med* 2022;28:2155–61.
8 Cascone T, William WN Jr, Weissferdt A, *et al*. Neoadjuvant nivolumab or nivolumab plus ipilimumab in operable non-small cell lung cancer: the phase 2 randomized NEOSTAR trial. *Nat Med* 2021;27:504–14.
9 Ready N, Tong B, Clarke J, *et al*. P2.04-89 Neoadjuvant Pembrolizumab in Early Stage Non-Small Cell Lung Cancer (NSCLC): Toxicity, Efficacy, and Surgical Outcomes. *J Thorac Oncol* 2019;14:S745.
10 Deng H, Zhao Y, Cai X, *et al*. PD-L1 expression and Tumor mutation burden as Pathological response biomarkers of Neoadjuvant immunotherapy for Early-stage Non-small cell lung cancer: A systematic review and meta-analysis. *Crit Rev Oncol Hematol* 2022;170:103582.
11 Roulleaux Dugage M, Albarrán-Artahona V, Laguna JC, *et al*. Biomarkers of response to immunotherapy in early stage non-small cell lung cancer. *Eur J Cancer* 2023;184:179–96.
12 Tong BC, Gu L, Wang X, *et al*. Perioperative outcomes of pulmonary resection after neoadjuvant pembrolizumab in patients with non–small cell lung cancer. *J Thorac Cardiovasc Surg* 2022;163:427–36.
13 Schefzik R, Flesch J, Goncalves A. Fast identification of differential distributions in single-cell RNA-sequencing data with waddR. *Bioinformatics* 2021;37:3204–11.
14 Dharmaratne M, Kulkarni AS, Taherian Fard A, *et al*. scShapes: a statistical framework for identifying distribution shapes in single-cell RNA-sequencing data. *Gigascience* 2022;12:giac126.
15 Zhang M, Guo FR. BSDE: barycenter single-cell differential expression for case-control studies. *Bioinformatics* 2022;38:2765–72.
16 Zhang J, Li J, Lin L. Statistical and machine learning methods for immunoprofiling based on single-cell data. *Hum Vaccin Immunother* 2023;19:2234792.
17 Wood C, Lyniv L, Isaacs JM, *et al*. Perioperative pembrolizumab in early-stage non-small cell lung cancer (NSCLC): safety, efficacy, and exploratory biomarker analysis. *J Immunother Cancer* 2025;13:e010395.
18 Baldan V, Griffiths R, Hawkins RE, *et al*. Efficient and reproducible generation of tumour-infiltrating lymphocytes for renal cell carcinoma. *Br J Cancer* 2015;112:1510–8.
19 Haghverdi L, Lun ATL, Morgan MD, *et al*. Batch effects in single-cell RNA-sequencing data are corrected by matching mutual nearest neighbors. *Nat Biotechnol* 2018;36:421–7.
20 Chan C, Feng F, Ottinger J, *et al*. Statistical mixture modeling for cell subtype identification in flow cytometry. *Cytometry A* 2008;73:693–701.
21 Lo K, Brinkman RR, Gottardo R. Automated gating of flow cytometry data via robust model-based clustering. *Cytometry A* 2008;73:321–32.
22 Pyne S, Hu X, Wang K, *et al*. Automated high-dimensional flow cytometric data analysis. *Proc Natl Acad Sci U S A* 2009;106:8519–24.
23 Lin L, Chan C, West M. Discriminative variable subsets in Bayesian classification with mixture models, with application in flow cytometry studies. *Biostatistics* 2016;17:40–53.
24 Lin L, Hejblum BP. Bayesian mixture models for cytometry data analysis. *WIREs Computational Stats* 2021;13:e1535.
25 Lin L, Shi W, Ye J, *et al*. Multisource single-cell data integration by MAW barycenter for Gaussian mixture models. *Biometrics* 2023;79:866–77.
26 Alekseyenko AV. Multivariate Welch t-test on distances. *Bioinformatics* 2016;32:3552–8.
27 Hill S, Sugiyarto G, Harrington J, *et al*. High proportion of PD-1 and CD39 positive CD8+ tissue resident T lymphocytes correlates with better clinical outcomes in resected human oesophageal adenocarcinoma. *Cancer Immunol Immunother* 2024;73:213.
28 Palomero J, Panisello C, Lozano-Rabella M, *et al*. Biomarkers of tumor-reactiove $CD4^+$ and CD8+ TILS associate with improved prognosis in endometrial cancer. *J Immunother Cancer* 2020.
29 Duhen T, Duhen R, Montler R, *et al*. Co-expression of CD39 and CD103 identifies tumor-reactive CD8 T cells in human solid tumors. *Nat Commun* 2018;9:2724.
30 Attrill GH, Owen CN, Ahmed T, *et al*. Higher Proportions of CD39+ tumor-resident cytotoxic T cells predict recurrence-free survival in patients with stage III melanoma treated with adjuvant immunotherapy. *J Immunother Cancer* 2022;10:1–15.
31 Romagnoli G, D'Alessandris QG, Capone I, *et al*. CD8+CD103+PD1+TIM3+ T cells in glioblastoma microenvironment correlate with prognosis. *Immunology* 2024;171:198–211.
32 Vlaming M, Bilemjian V, Freile JÁ, *et al*. Tumor infiltrating CD8/CD103/TIM-3-expressing lymphocytes in epithelial ovarian cancer co-express CXCL13 and associate with improved survival. *Front Immunol* 2022;13.
33 Miller BC, Sen DR, Al Abosy R, *et al*. Subsets of exhausted CD8+ T cells differentially mediate tumor control and respond to checkpoint blockade. *Nat Immunol* 2019;20:326–36.
34 Tassi E, Bergamini A, Wignall J, *et al*. Epithelial ovarian cancer is infiltrated by activated effector T cells co-expressing CD39, PD-1, TIM-3, CD137 and interacting with cancer cells and myeloid cells. *Front Immunol* 2023;14.
35 Clarke J, Panwar B, Madrig R. Single-cell transcriptomic analysis of tissue-resident memory T cells in human lung cancer. *J Exp Med* 2019;216:2128–49.
36 Gautron A-S, Dominguez-Villar M, de Marcken M, *et al*. Enhanced suppressor function of TIM-3+ FoxP3+ regulatory T cells. *Eur J Immunol* 2014;44:2703–11.
37 Palermo B, Franzese O, Frisullo G, *et al*. CD28/PD1 co-expression: dual impact on $CD8^+$ T cells in peripheral blood and tumor tissue, and its significance in NSCLC patients' survival and ICB response. *J Exp Clin Cancer Res* 2023;42:287.
38 He H, Qiao B, Guo S, *et al*. Interleukin-7 regulates CD127 expression and promotes $CD8^+$ T cell activity in patients with primary cutaneous melanoma. *BMC Immunol* 2022;23:35.
39 Ichiki Y, Fukuyama T, Ueno M, *et al*. Immune profile analysis of peripheral blood and tumors of lung cancer patients treated with immune checkpoint inhibitors. *Transl Lung Cancer Res* 2022;11:2192–207.
40 Miao K, Zhang X, Wang H, *et al*. Peripheral blood lymphocyte subsets predict the efficacy of immune checkpoint inhibitors in non-small lung cancer. *Front Immunol* 2022.
41 Chin WL, Cook AM, Chee J, *et al*. Coupling of response biomarkers between tumor and peripheral blood in patients undergoing chemoimmunotherapy. *Cell Rep Med* 2025;6:101882.
42 Marcos Rubio A, Everaert C, Van Damme E, *et al*. Circulating immune cell dynamics as outcome predictors for immunotherapy in non-small cell lung cancer. *J Immunother Cancer* 2023;11:e007023.
43 Kim GD, Shin S-I, Sun P, *et al*. Single-cell RNA sequencing of baseline PBMCs predicts ICI efficacy and irAE severity in patients with NSCLC. *J Immunother Cancer* 2025;13:e011636.